

16. C. I. Fassett, J. W. Head III, *Icarus* **195**, 61 (2008).
 17. B. A. Cohen, T. D. Swindle, D. A. Kring, *Science* **290**, 1754 (2000).
 18. G. Neukum, B. A. Ivanov, W. K. Hartmann, *Space Sci. Rev.* **96**, 55 (2001).
 19. R. G. Strom, R. Malhotra, T. Ito, F. Yoshida, D. A. Kring, *Science* **309**, 1847 (2005).
 20. W. K. Hartmann, *Meteoritics* **30**, 451 (1995).
 21. *R* plots are constructed by dividing the differential SFD by a power law $dN/dD \sim D^{-3}$, where *N* is the number of craters within a given increment of crater diameter in a given area (18).
 22. We thank the LRO and LOLA mission teams for their efforts, which made the observations

in this study possible, and T. Kneissl for developing the CraterTools extension to ArcMap. Funding was provided by NASA grant NNX09AM54G for LOLA.

13 July 2010; accepted 25 August 2010
 10.1126/science.1195050

Global Silicate Mineralogy of the Moon from the Diviner Lunar Radiometer

Benjamin T. Greenhagen,^{1*} Paul G. Lucey,² Michael B. Wyatt,³ Timothy D. Glotch,⁴ Carlton C. Allen,⁵ Jessica A. Arnold,⁴ Joshua L. Bandfield,⁶ Neil E. Bowles,⁷ Kerri L. Donaldson Hanna,³ Paul O. Hayne,⁸ Eugenie Song,⁶ Ian R. Thomas,⁷ David A. Paige⁸

We obtained direct global measurements of the lunar surface using multispectral thermal emission mapping with the Lunar Reconnaissance Orbiter Diviner Lunar Radiometer Experiment. Most lunar terrains have spectral signatures that are consistent with known lunar anorthosite and basalt compositions. However, the data have also revealed the presence of highly evolved, silica-rich lunar soils in kilometer-scale and larger exposures, expanded the compositional range of the anorthosites that dominate the lunar crust, and shown that pristine lunar mantle is not exposed at the lunar surface at the kilometer scale. Together, these observations provide compelling evidence that the Moon is a complex body that has experienced a diverse set of igneous processes.

Remote characterization of mineralogy through thermal emission spectroscopy has a long history in planetary science that recently has been highlighted by global maps of martian mineralogy obtained from orbit and measurements from the martian surface (1, 2). Although infrared emission spectroscopy is sensitive to the bulk composition and can readily identify important lunar silicates such as feldspar, pyroxene, olivine, and quartz (3), earlier lunar observations (4, 5) lacked sufficient spatial resolution or coverage to identify areas that may have escaped extensive physical mixing and retain unusual lithologies. High-resolution lunar mapping has thus far been limited to visible and near-infrared spectroscopy and multispectral imaging, which have been used to identify diverse compositions over large areas of the lunar surface (6–9). However, these techniques are relatively insensitive to nominally iron-free minerals such as quartz and feldspar and can only unambiguously detect the important lunar rock-type anorthosite in exposures that contain almost no mafic minerals, such as pyroxene or olivine (9). Multispectral thermal emission data from the Diviner lunar radiometer have high spatial

resolution, near global coverage, and sensitivity to important iron-poor mineralogy.

Launched onboard the Lunar Reconnaissance Orbiter (LRO) in June 2009, Diviner is a nine-channel pushbroom mapping radiometer that measures emitted thermal radiation (seven channels) and reflected solar radiation (two channels) between 0.3 and 400 μm at a spatial resolution of approximately 200 m (10). The Diviner compositional investigation relies primarily on the three shortest wavelength thermal infrared channels near 8 μm : 7.55 to 8.05 μm , 8.10 to 8.40 μm ,

and 8.38 to 8.68 μm . Pioneering lunar mid-infrared spectroscopic studies, including airborne (4), ground-based (5), and laboratory (11–13) measurements, have shown this region is key to identifying common lunar silicate minerals, and the Diviner compositional investigation was designed by using the results of those studies (14).

We chose Diviner's 8- μm -region channels to characterize a well-studied compositional indicator of silicate mineralogy called the Christiansen feature (CF) (14, 15). The wavelength position of CF is strongly dependent on the degree of polymerization of minerals, with framework silicate minerals such as feldspars exhibiting CFs at shorter wavelengths than less polymerized pyroxene and olivine (3, 16, 17). Common lunar minerals thus exhibit widely separated CF positions. The CF position of soils is close to the weighted average of the constituent minerals, which enables determination of major lunar lithologies (18). The presence of strong thermal gradients in the lunar environment causes systematic shifts in CF position and an enhancement of CF spectral contrast relative to other mid-infrared features, such as Reststrahlen bands (3, 19, 20). Therefore, lunar thermal emission observations are only directly comparable with laboratory emission measurements in a simulated lunar environment (21, 22).

We used $\sim 10^8$ three-point 8- μm -region spectra collected between 5 August 2009 and 24 November 2009, covering $\sim 50\%$ of the lunar surface

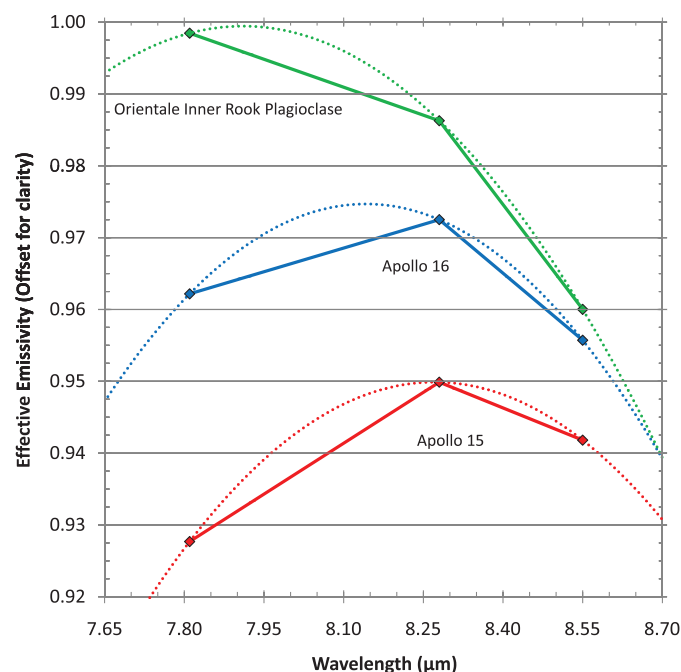


Fig. 1. Diviner 8- μm -region channel three-point spectra representing typical spectral variability. The CF position was determined by using a parabolic fit to the three points (dotted traces).

¹Jet Propulsion Laboratory, California Institute of Technology, Pasadena, CA 91109, USA. ²Hawaii Institute of Geophysics and Planetology, University of Hawaii, Honolulu, HI 96822, USA. ³Department of Geological Sciences, Brown University, Providence, RI 02912, USA. ⁴Department of Geosciences, Stony Brook University, Stony Brook, NY 11794, USA. ⁵NASA Johnson Space Center, Houston, TX 77058, USA. ⁶Department of Earth and Space Sciences, University of Washington, Seattle, WA 98195, USA. ⁷Department of Atmospheric, Oceanic, and Planetary Physics, Oxford University, OX1 3PU Oxford, UK. ⁸Department of Earth and Space Sciences, University of California, Los Angeles, Los Angeles, CA 90095, USA.

*To whom correspondence should be addressed. E-mail: benjamin.t.greenhagen@jpl.nasa.gov

between 60°N and 60°S. The field of view of the instrument causes spatial gaps between orbit tracks as collected to date; however, Diviner has comprehensively sampled all major lunar terrains and continues to increase spatial coverage as the LRO mission proceeds. To characterize silicate mineralogy from Diviner spectra, we first binned and averaged calibrated radiance at 32 pixels per degree (~1 km per pixel at the equator), calculated an effective emissivity for each channel, and then estimated the position of the CF using a parabolic fit to the three channels (Fig. 1) (16). High-spectral-resolution laboratory experiments have shown that a parabola is a good approximation for the shape of the CF across this restricted wavelength range (11, 16, 21, 22).

We analyzed Diviner 8- μ m-region spectra to determine the maxima of parabolic fits ("CF values") and assembled the result into a comprehensive map of lunar silicate mineralogy (Fig. 2). The data were corrected to remove temperature effects, including anisothermality (topographically driven subpixel variations in temperature) (16). Over 90% of the CF values are between 8.04 and 8.36 μ m (Fig. 3). The known mineralogical differences between basaltic maria with abundant pyroxene and the feldspathic highlands, which are rich in plagioclase feldspar, are readily apparent. The observed variability in CF values is also influenced by space weathering, which is the re-orientation of the lunar surface to exposure to micrometeorites and solar wind sputtering (23). The space-weathering effect was not anticipated (18) and shifts CF values to longer wavelengths with increasing maturity (longer exposure time on the surface) relative to fresh "immature" surfaces (16).

Diviner observations are consistent with previous regional lunar surface observations (4) and are directly comparable with laboratory measurements of returned lunar soils in a simulated lunar environment (12, 13, 16). The mean CF values for highland-dominated areas are shorter than those for the mare-dominated areas, which are consistent with the mineralogical differences between the feldspar-rich lunar highlands of the Apollo 16 landing site and the feldspar-poor lunar maria of the Apollo 11, 12, 15, and 17 landing sites (Fig. 4) (24, 25). The Apollo 14 site, which is dominated by mafic basin ejecta, has an intermediate mean CF value. Although most Diviner observations fall within the range of typical highlands and maria, there are locations with unusual CF positions, 8- μ m-region spectral signatures, or both.

In restricted regions that have previously been shown to exhibit unusually high abundances of the incompatible element thorium (26), there is evidence of highly silicic material: quartz, silica glass of similar composition, or sodium- or potassium-rich (or both) varieties of feldspar. These minerals are indicators of extremely differentiated lunar rocks, including granites. Diviner data associated with these kilometer-scale or larger exposures, and laboratory measurements of similar materials in simulated lunar environment, exhibit distinct spectral characteristics owing to CF positions well

shortward of the 8- μ m-region channels' wavelength range (21, 22). Prior work had highlighted some of these locations (lunar red spots) because of their unusual morphologies and anomalous ultraviolet ratios and because of their unusually high thorium values (27–30). However, a definitive compositional diagnosis required direct detection of the indicator minerals. Glotch *et al.* (22) have used Diviner data to perform a comprehensive survey of the lunar red spots and identify Hansteen Alpha, Lassell Massif, the Gruithuisen Domes, and Aristarchus Crater as high-silica features. Because the volume of silicic rock relative to a basaltic precursor is small, simple extreme differentiation of a basaltic magma raises issues of storage and heat supply to such large magma bodies. This suggests that basaltic intrusive magmatism may have remelted and subsequently differentiated a previously more silica-rich precursor, such as anorthositic crust (22). Alternatively, it is possible that the thorium-rich, high-silica features may represent direct ex-

trusive examples of the incompatible element-rich residual liquids from the lunar magma ocean.

The silica-rich red spots are confined to a large region on the lunar nearside called the Procellarum KREEP (for potassium, rare earth elements, and phosphorous) Terrane (PKT), where most of the surface thorium on the Moon is found, and the presence of high concentrations of heat-producing elements is invoked to account for the extensive basaltic volcanism on the lunar nearside (31). This regionally concentrated heat source plausibly enabled the differentiation that gave rise to the silicic anomalies. However, we also detected high amounts of silica outside the PKT in the Compton Belkovich thorium anomaly on the lunar far side. Recent Lunar Reconnaissance Orbiter Camera images show that this location is a low dome, with unusual morphologies revealed at the 10-m scale (32). Therefore, whatever process gave rise to these silicic features either did not require the special thermal conditions of the PKT (such

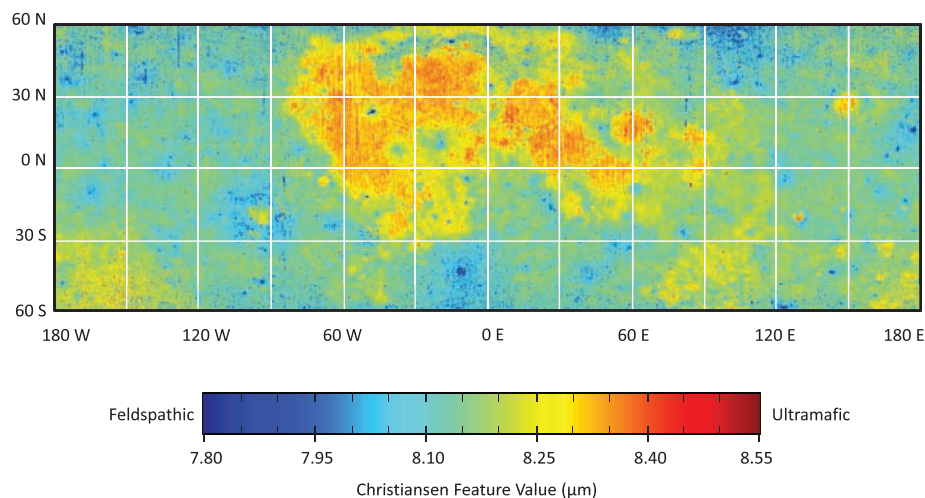


Fig. 2. CF value map of silicate mineralogy. The color map was chosen to highlight compositional variability of common lunar terrains and saturate blue or red for unusual compositions (Fig. 3). This map uses a pyramidal spatial resolution structure between 8 and 0.5 pixels per degree.

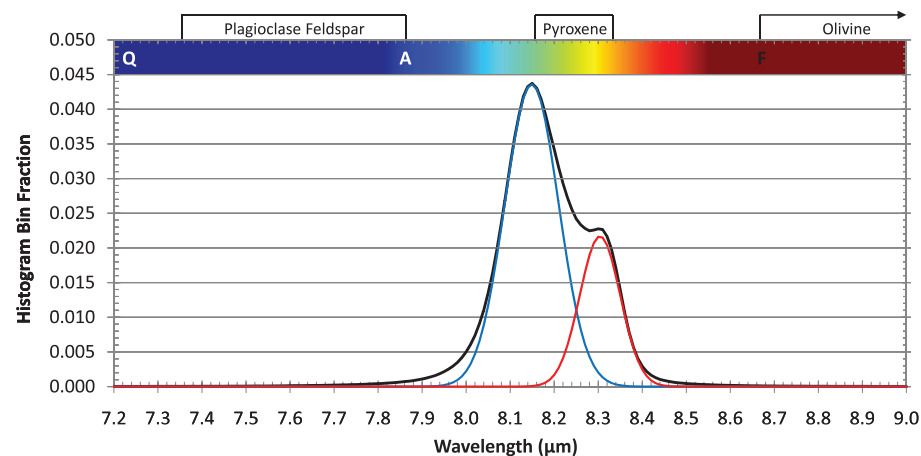


Fig. 3. Histogram of Diviner CF values between 30°N and 30°S. Diviner CF values (black trace) have a bimodal distribution with modal means for highland (blue trace) and mare (red trace) compositions of 8.15 and 8.30 μ m, respectively. CF positions were measured in simulated lunar conditions for relevant minerals (A, anorthite; F, forsterite; and Q, quartz), and ranges for mineral types are included.

as whether it is a direct magma ocean product), or the PKT is much more extensive but its thorium is sequestered at depth, which is in contrast to prior interpretations that suggested the far-side thorium had been depleted (26).

We have also identified a class of anomalous kilometer-scale exposures with CF values between those of the high silica features and those of the extraordinarily calcium-rich anorthite that is well known from anorthosites in the lunar sample collection. This class of feature (“intermediate composition plagioclase”) is consistent with plagioclase compositions such as bytownite or labradorite, which are somewhat more sodium-rich than the crust-forming ferroan anorthosites (Fig. 3) (14). Unlike the high-silica features, these plagioclase features have CF positions near the 8- μ m-region channels (thus enabling the determination of a CF value) and are not correlated with thorium anomalies. The CF value difference between the intermediate plagioclase composition features (for example, Guthnick crater in the southern highlands has a mean CF value of 7.68 μ m) and immature crystalline anorthite measured in a simulated lunar environment (7.84 μ m for An90) is large and is of similar magnitude to the difference in modal CF values of highlands and maria (16, 21, 22).

The intermediate composition plagioclase features occur in a wide range of lunar terrains. We found that 15 of the areas previously shown to be pure plagioclase feldspar on the basis of near-infrared spectroscopy (9) show evidence for intermediate composition plagioclase and that an additional 19 of the areas have either extremely immature pure anorthite or are mature or mixed intermediate composition plagioclase, or both (16). The detection of widespread intermediate composition plagioclase indicates that the lunar crust may have localized variations in plagioclase composition. Anorthosites with approximately these compositions are known in the sample collection (such as the alkali anorthosites), but all of these are rich in incompatible elements and may not be related to the thorium-poor locations we have identified (33). The intermediate composition plagioclase may thus reflect geochemical heterogeneities

and variable cooling within the lunar magma ocean or secondary processing of an early lunar crust.

There is no evidence of olivine-rich ultramafic lithologies, including any that might indicate the presence of kilometer-scale exposures of lunar mantle at the surface. Using the same methodology we used to directly detect high-silica features (extreme mean CF values and distinct character owing to CF positions well outside the 8- μ m-region channels’ wavelength range), we failed to detect any contiguous regions with very long wavelength CF positions. Most of the proposed lunar mantle compositions contain little or no feldspar, being dominated by pyroxene, olivine, or both (34), and such ultramafics would be readily identified by Diviner (16). Given our current constraints in latitude, spatial coverage, and spatial resolution, we found no exposures that have CF values longer than typical lunar maria, which contain tens of percent plagioclase feldspar. Rare individual 1/32-degree pixels are detected with these characteristics, but in the absence of other evidence we attribute these occurrences to processing errors caused by shadows, topographic relief, or both (16). A recent inspection of full-resolution Diviner data for central peaks and other locations that have been previously suggested to reveal uplifted ultramafic compositions on the basis of multispectral near-infrared data (7) also revealed no evidence of surfaces dominated by olivine-rich ultramafic lithologies (35).

Our study includes the interior of the vast South Pole Aitken basin, which is large enough to have penetrated through the crust and into the mantle (36). If the basin did excavate mantle material, the upper surface is extensively mixed with more feldspathic crustal rocks from the many basins and lesser impacts into the ancient South Pole Aitken basin, and no pristine exposures are found at the kilometer scale. Recently, Yamamoto *et al.* (37) have reported possible mantle outcrops in several regions on the Moon. Although we have not compared their reported locations directly, our coverage includes all of their study areas. Our results suggest that if the Yamamoto *et al.* (37) detections include mantle material, it must be

mixed with feldspathic material to have eluded detection by Diviner. The search for lunar mantle is a prime example of the complementary nature of near infrared and thermal infrared spectroscopy with respective sensitivities to iron-rich and iron-poor mineralogy.

References and Notes

- J. L. Bandfield *et al.*, *Science* **287**, 1626 (2000).
- P. R. Christensen *et al.*, *Science* **306**, 1733 (2004).
- J. W. Salisbury, L. S. Walter, *J. Geophys. Res.* **94**, (B7), 9192 (1989).
- F. H. Murcray, D. G. Murcray, W. J. Williams, *J. Geophys. Res.* **75**, 2662 (1970).
- A. L. Sprague *et al.*, *Icarus* **115**, 181 (1992).
- C. M. Pieters, *Rev. Geophys.* **24**, 557 (1986).
- S. Tompkins, C. M. Pieters, *Meteorit. Planet. Sci.* **34**, 25 (1999).
- P. G. Lucey, *Geophys. Res. Lett.* **31**, L08701 (2004).
- M. Ohtake *et al.*, *Nature* **461**, 236 (2009).
- D. A. Paige *et al.*, *Space Sci. Rev.* **150**, 125 (2010).
- L. M. Logan, G. R. Hunt, J. W. Salisbury, S. R. Balsamo, *J. Geophys. Res.* **78**, 4983 (1973).
- J. W. Salisbury *et al.*, *Proc. Lunar Planet. Sci. Conf.* **4**, 3191 (1973).
- L. M. Logan *et al.*, in *Infrared and Raman Spectroscopy of Lunar and Terrestrial Minerals*, C. Karr, Ed. (Academic Press, New York, 1975), pp. 117–142.
- B. T. Greenhagen, *Ph.D. Dissertation*, UCLA (2009).
- J. E. Conel, *J. Geophys. Res.* **74**, 1614 (1969).
- Materials and methods are available as supporting material on Science Online.
- W. B. White, in *Infrared and Raman Spectroscopy of Lunar and Terrestrial Minerals*, C. Karr, Ed. (Academic Press, New York, 1975), pp. 325–358.
- D. B. Nash, J. W. Salisbury, J. E. Conel, P. G. Lucey, P. R. Christensen, *J. Geophys. Res.* **98**, 23535 (1993).
- L. M. Logan *et al.*, *Proc. Lunar Planet. Sci. Conf.* **3**, 3191 (1972).
- B. G. Henderson, P. G. Lucey, B. M. Jakosky, *J. Geophys. Res.* **101**, 14969 (1996).
- I. R. Thomas *et al.*, *Proc. Lunar Planet. Sci. Conf.* **41**, 1364 (2010).
- T. D. Glotch *et al.*, *Science* **329**, 1510 (2010).
- B. Hapke, *J. Geophys. Res.* **106**, 10039 (2001).
- L. A. Taylor, C. M. Pieters, L. P. Keller, R. V. Morris, D. S. McKay, *J. Geophys. Res.* **106**, 27985 (2001).
- L. A. Taylor *et al.*, *J. Geophys. Res.* **115**, E00E15 (2010).
- D. J. Lawrence *et al.*, *J. Geophys. Res.* **108**, 5102 (2003).
- E. A. Whitaker, *Moon* **4**, 348 (1972).
- J. W. Head 3rd, T. B. McCord, *Science* **199**, 1433 (1978).
- B. C. Bruno *et al.*, *Proc. Lunar Planet. Sci. Conf.* **21**, 405 (1991).
- J. J. Hagerty *et al.*, *J. Geophys. Res.* **111**, E06002 (2006).
- M. A. Wicczorek, R. J. Phillips, *J. Geophys. Res.* **105**, 20417 (2000).
- B. L. Jolliff *et al.*, *Proc. Lunar Planet. Sci. Conf.* **41**, 2412 (2010).
- J. W. Shervais, J. J. McGee, *Am. Mineral.* **84**, 806 (1999).
- C. K. Shearer, J. J. Papike, *Am. Mineral.* **84**, 1469 (1999).
- E. Song *et al.*, *Proc. Lunar Planet. Sci. Conf.* **41**, 2578 (2010).
- P. G. Lucey, G. J. Taylor, B. R. Hawke, P. D. Spudis, *J. Geophys. Res.* **103**, 3701 (1998).
- S. Yamamoto *et al.*, *Nat. Geosci.* **3**, 533 (2010).
- This research was carried out in part at the Jet Propulsion Laboratory, California Institute of Technology, under a contract with NASA. This work was funded by the Diviner science budget and the NASA LRO Participating Scientist program.

Supporting Online Material

www.sciencemag.org/cgi/content/full/329/5998/1507/DC1

Materials and Methods

SOM Text

Figs. S1 to S3

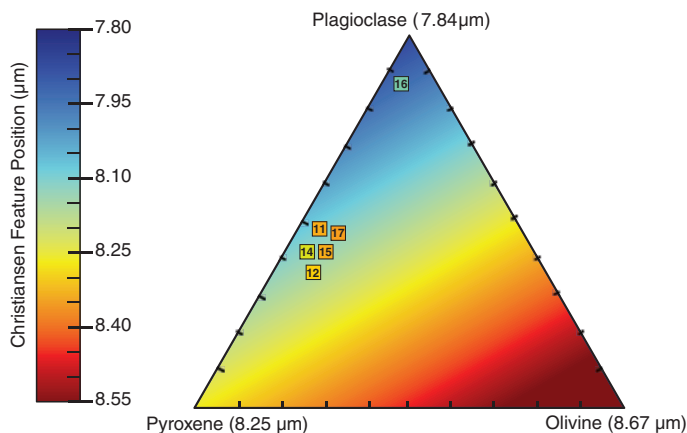
Table S1

References

12 May 2010; accepted 1 September 2010

10.1126/science.1192196

Fig. 4. Silicate ternary with CF values. This ternary was constructed by using CF positions for crystalline immature plagioclase (anorthite endmember), pyroxene (intermediate composition), and olivine (forsterite endmember) measured in simulated lunar conditions and assuming a linear mixing behavior for the CF position (18). The ternary location for a representative soil sample and mean CF value from each Apollo site are superimposed.



This copy is for your personal, non-commercial use only.

If you wish to distribute this article to others, you can order high-quality copies for your colleagues, clients, or customers by [clicking here](#).

Permission to republish or repurpose articles or portions of articles can be obtained by following the guidelines [here](#).

The following resources related to this article are available online at www.sciencemag.org (this information is current as of October 12, 2015):

Updated information and services, including high-resolution figures, can be found in the online version of this article at:

<http://www.sciencemag.org/content/329/5998/1507.full.html>

Supporting Online Material can be found at:

<http://www.sciencemag.org/content/suppl/2010/09/14/329.5998.1507.DC1.html>

A list of selected additional articles on the Science Web sites **related to this article** can be found at:

<http://www.sciencemag.org/content/329/5998/1507.full.html#related>

This article **cites 33 articles**, 6 of which can be accessed free:

<http://www.sciencemag.org/content/329/5998/1507.full.html#ref-list-1>

This article has been **cited by** 3 articles hosted by HighWire Press; see:

<http://www.sciencemag.org/content/329/5998/1507.full.html#related-urls>

This article appears in the following **subject collections**:

Planetary Science

http://www.sciencemag.org/cgi/collection/planet_sci